JOURNAL OF MATERIALS SCIENCE 37 (2002) 59–64

A study of grain-boundary structure in rare-earth doped aluminas using an EBSD technique

J. CHO, C.-M. WANG, H. M. CHAN, J. M. RICKMAN, M. P. HARMER
Materials Research Center, Whitaker Laboratory,
Lehigh University, Bethlehem, PA 18015, USA
E-mail: HMC0@Lehigh.edu

Oversized rare-earth dopant ions such as Y^{3+}, Nd^{3+}, and La^{3+} segregate to grain boundaries and reduce the tensile creep rate of α-Al_2O_3 by 2-3 orders of magnitude. It has been speculated that these dopant ions can modify the grain boundary structure in alumina by promoting the formation of special grain boundaries. If this were indeed the case, it would provide a possible explanation for the aforementioned creep rate retardation. In order to test this hypothesis, electron backscatter diffraction (EBSD) has been used to assess both the proportion of coincidence-site lattice boundaries, and the grain boundary misorientation distribution, in aluminas doped with various ions (Zr, Y, Nd, La, Nd/Zr). The results show that the grain boundary structure in alumina is not significantly altered by the addition of the above dopants, implying that the change in grain boundary chemistry is primarily responsible for the observed creep behavior.

1. Introduction

It has been found that the tensile creep rate of α-Al_2O_3 is reduced by 2-3 orders of magnitude with the addition of ppm levels of oversized, isovalent dopant ions (e.g., Y^{3+}, Nd^{3+}, La^{3+}) [1–3]. Due to the dramatic creep improvement, these doped oxide systems can be utilized in ceramic matrix composites (CMCs) intended for very high temperature environments (e.g., $>1400°C$), where oxidation is of major concern [4–6]. In these promising materials, emerging evidence suggests that grain boundaries play a dominant role in this behavior, however the detailed nature of the mechanism responsible for the creep enhancement is the subject of debate. Previous work has shown that the dopants strongly segregate to grain boundaries, driven by their large size (radius) mismatch between the dopant ions (Y^{3+}: 0.89 Å, Nd^{3+}: 0.99 Å, La^{3+}: 1.06 Å), and the host Al^{3+} (0.51 Å) [7–10]. It was suggested by Cho *et al*. that the observed reductions in creep rate resulted from a 'site-blocking' effect of oversized segregant ions on selected grain boundary diffusion paths [2]. Recent determinations of Al^{3+} migration enthalpies by computer simulations support this idea, but direct experimental evidence is scarce [11].

Recently, Yoshida *et al*. [12] have studied the effectiveness of a series of lanthanide oxides (Sm, Eu, Tm, Lu) on the creep rate of alumina. They found that the effectiveness of the dopants in retarding creep was in the order, Sm < Tm < Eu < Lu, (although it should be mentioned that the data were not corrected to take into account the effect of grain size). Yoshida and coworkers explained the trend in creep behavior in terms of the effect of the dopant on the chemical bond strength around the A1 ion, based on first principles molecular orbital calculations. According to the "site-blocking" model one would have predicted the opposite trend, since Lu has the smallest ionic radius (0.861 Å) and Sm has the largest (0.96 Å).

Another possibility is that the presence of the dopant ions can modify the grain boundary structure. The argument is that certain types of 'special' boundaries are favored, which play a limiting role in the transmission of grain boundary sliding during creep deformation, due to the difficulty in accommodating lattice dislocations [13, 14]. Lartigue and Priester [15] reported that a dopant ion such as magnesium (Mg) increased the proportion of special (i.e., coincidence site lattice-CSL and coincidence axis direction-CAD) grain boundaries in alumina. In subsequent work, however, Lartigue-Korinek and Dupau [16] observed that yttrium addition leads to a proportion of near coincident boundaries which is close to that found in undoped alumina. In addition, Bouchet *et al*. [17] have shown that there is a relationship between grain boundary plane orientation and Y segregation, and argued that Y segregated grain boundaries are indeed flat and have ordered structures on the atomic scale.

In contrast to the above model, recent studies by Cho *et al*. using electron back-scatter diffraction (EBSD) [18] and Gülgün *et al*. using TEM [19], did not reveal any significant differences in grain boundary structure between Y-doped alumina and undoped alumina. The aim of the present work was to extend our previous EBSD study to other dopant systems (Zr, Nd, La, Nd/Zr) which have also resulted in enhanced creep behavior [1–3], and hence elucidate the beneficial role of

these ions. Based on previous work [18] where it was found that the misorientation distribution in Y-doped crept samples was essentially identical to that of the undeformed samples, all of the EBSD characterization in the present study was carried out on as hot-pressed specimens. Note that data from the Y-doped sample is included not only for completeness, but also because the previous study utilized *hexagonal* rather than *rhombohedral* symmetry. It is also worth mentioning that the EBSD technique [20, 21] has several advantages over the TEM; most importantly, it can characterize a large number of grains in a single scan, and in addition specimen preparation is relatively easy.

2. Experimental procedure

2.1. Specimen preparation

For the investigation of grain orientation and grain boundary geometry (i.e. misorientation angle and axis), six alumina specimens were examined; undoped alumina (Pure A), 1000 ppm Y-doped alumina (YA), 500 ppm La-doped alumina (LA), 100 ppm Nd-doped alumina (ND), 100 ppm Zr-doped alumina (ZR), and 100/100 ppm Nd/Zr-codoped alumina. In all cases, the purity of the starting alumina powder (AKP-53, Sumitomo Chemical America, New York, NY) was 99.995%. A broad range of dopant concentrations was purposely selected in an effort to test the general applicability of the observed results. Note that a similar approach was adopted in previous creep studies to test dopant levels both below and above the solubility limit [22]. All six specimens were hot-pressed, and the processing conditions of these materials have been described elsewhere [1–3, 9]. For EBSD observation, the surfaces of the as-hot-pressed specimens were polished down to a 1 μm finish with diamond slurry, followed by polishing with 0.02 μm colloidal SiO_2 in the vibratory polisher (Vibromet II, Buehler, Lake Bluff, IL). In order to avoid charging, a thin carbon layer (<5 nm) was deposited on the polished surface.

2.2. Acquisition of EBSD patterns

The details of the SEM operation conditions and EBSD acquisition were described in previous studies [11, 18]. Essentially, diffraction of the backscattered electrons occurs, where for a given set of crystal planes, the directions of the diffraction maxima define a pair of cones, directed away from either side of the crystal plane. When projected onto a flat screen, the pairs of cones appear as lines which define a Kikuchi band. The width of the band (i.e. the distance between lines of each pair) is inversely proportional to the d-spacing of the diffracting crystal plane, and the orientation of the band is determined by the spatial orientation of the crystal plane within the sample. The spatial resolution of backscattered electron diffraction is typically about 0.2 μm, with variations depending on the atomic number of the specimen and the accelerating voltage used in the SEM.

Subsequent analysis of the EBSD patterns using rhombohedral symmetry was carried out with the aid of computer software (TSL, Inc., Draper, UT). The stored data (location, orientation, and image quality) can be processed to create orientation imaging micrographs, thereby enabling a visual representation of the microstructure. Each location is represented by a pixel, to which a color or gray scale is assigned on the basis of grain orientation.

2.3. Analysis of EBSD results

The orientation of each grain is expressed with reference to a set of fixed orthogonal axes, one normal to the specimen plane, and two lying in the plane of the specimen. The detailed procedure for obtaining an absolute orientation from an EBSD pattern has been given in the literature [20, 23]. Briefly, the orientation is stored as a 3×3 matrix, which relates the crystal axis directions [100], [010], and [001] to the specimen directions. Given the orientation of each grain, the relative orientation between two contiguous grains, A1 and A2, is given by:

$$\mathrm{R12} = \mathrm{A1}^{-1}\mathrm{A2} \tag{1}$$

where R12 is the rotation matrix that represents rotation of A2 onto A1. The matrix, R12 can then be represented in terms of specific parameters such as ideal orientation, Euler angle, or angle and axis pair of rotation to convey orientation information [23]. In general, the angle/axis pair is used to describe the misorientation geometry between adjacent grains, and the smallest angle of the symmetry of rotation is chosen. Here, misorientations less than 5° were not searched, since low-angle boundaries are often difficult to distinguish from dislocation sub-boundaries. Note that although misorientations were determined using rhombohedral symmetry (which reflects the true three-fold rather than six-fold symmetry about the normal to the basal plane), for ease of recognition, the rotation axes in Table I are quoted with respect to indices corresponding to the hexagonal unit cell.

One advantage of the misorientation angle/axis concept is that it can readily be adapted to the CSL formalism. Thus, the 6 CSLs (Common rotations with $\Sigma = 36$)

TABLE I Selected CSLs with rotations about [00.1] and other directions [24]

Criterion	Σ	Misorientation (degrees)	uv.w
Common rotation	3	60.00	00.1
	7	38.21	00.1
	13	27.80	00.1
	19	46.83	00.1
	21	21.79	00.1
	31	17.90	00.1
Specific rotation	7	85.90	02.1
	11	95.22	01.0
	13	57.42	01.0
	17	96.76	12.1
	19	65.10	50.1
	21	64.62	11.0
	23	55.58	11.0
	31	56.74	50.2
	33	35.10	11.0
	36	86.02	02.1

for a rotation axis of [0001], as well as 10 CSLs for rotation axes of other direction (specific rotations with $\Sigma = 36$) were systematically searched based on the corresponding angle/axis pair (Table I) [24]. The crystal planes are indicated in Miller-Bravais notation of the non-primitive hexagonal lattice. Crystal directions are quoted using the convention commonly used for hexagonal unit cells: i.e., $[uvt \cdot w] \equiv [uv \cdot w]$, where $u + v + t = 0$ [24].

3. Results and discussion

Fig. 1 shows the EBSD derived orientation image maps (OIM) for undoped, Zr-doped, Y-doped, Nd-doped, La-doped and Nd/Zr-codoped aluminas; the grains are color coded, where each color corresponds to the orientation normal to the specimen surface, as represented in the stereographic triangle (Fig. 1g). In order to further explore texture information, the distribution of grain normals of the entire scanned area of the above

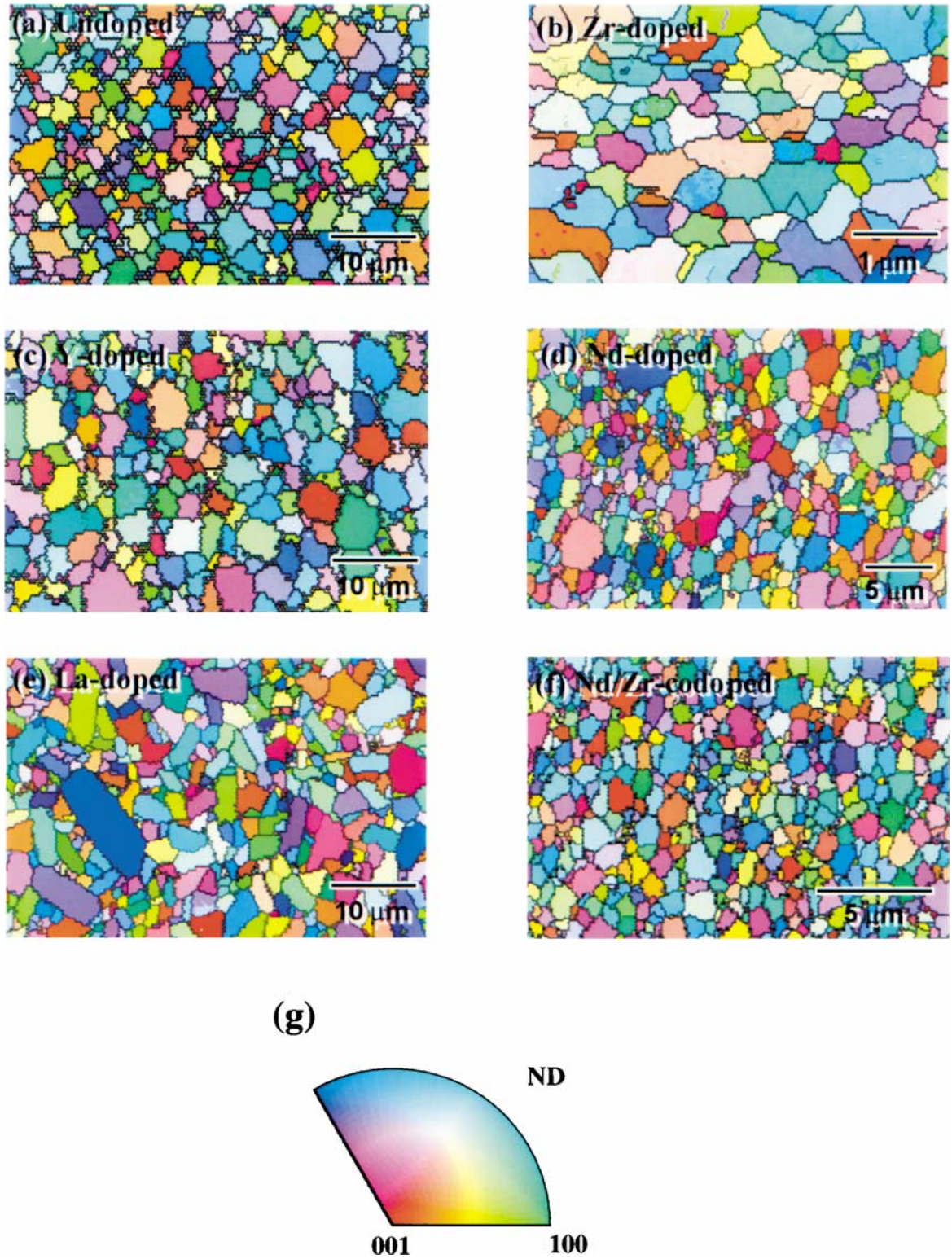

Figure 1 Orientation image maps (OIM) for (a) undoped alumina, compared with doped aluminas: (b) 100 ppm Zr; (c) 1000 ppm Y; (d) 100 ppm Nd; (e) 500 pm La; (f) 100/100 ppm Nd/Zr.

TABLE II EBSD acquisition parameters and grain size data

	Data points	Scan area (μm^2)	Step size (μm)	Total number of grains	Avg. grain diameter (μm)[a]
Pure A	29985	129.00 × 49.80	0.50	1610	2.25
ZR	23370	9.84 × 3.26	0.04	267	0.40
YA	34649	98.80 × 48.15	0.40	841	2.68
LA	36383	47.25 × 41.35	0.25	698	1.89
ND	48403	39.60 × 23.64	0.15	1029	1.08
NZ	49714	19.60 × 21.82	0.10	1475	0.61

[a]Average grain diameter = $2 \times \sqrt{A/\pi}$, where A = total area/total number of grains.

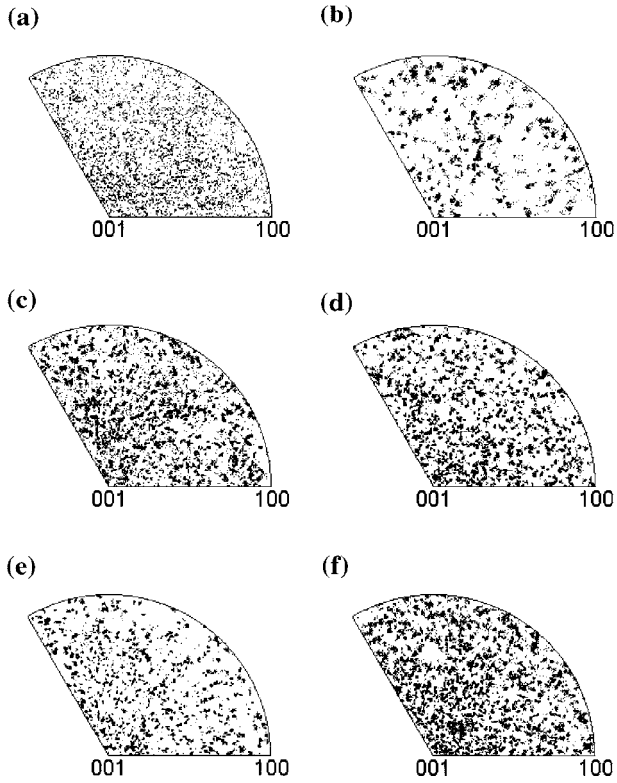

Figure 2 Inverse pole figures of grain normal directions for the entire scanned area of alumina specimens considered in Fig. 3: (a) undoped; (b) 100 ppm Zr; (c) 1000 ppm Y; (d) 100 ppm Nd; (e) 500 ppm La; (f) 100/100 ppm Nd/Zr.

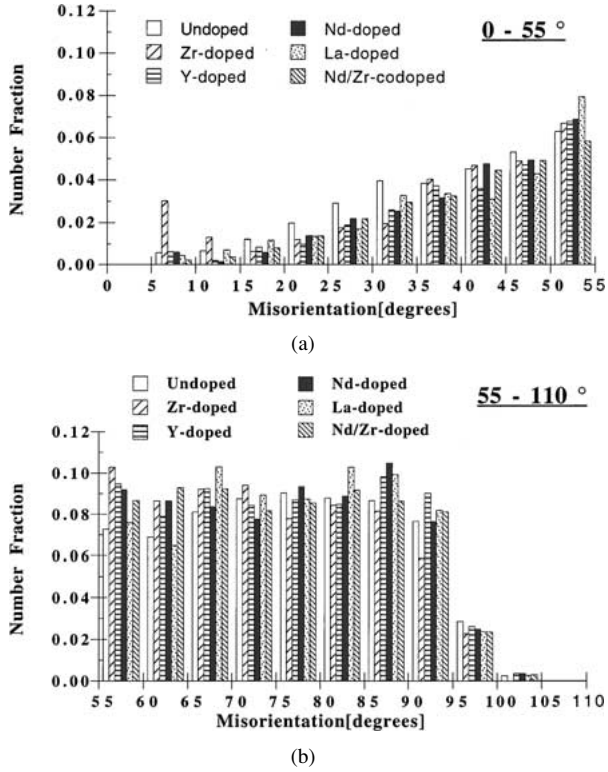

Figure 3 Misorientation angle histograms for undoped and various doped aluminas: (a) misorientation range of 5–55°; (b) misorientation range of 55–105°.

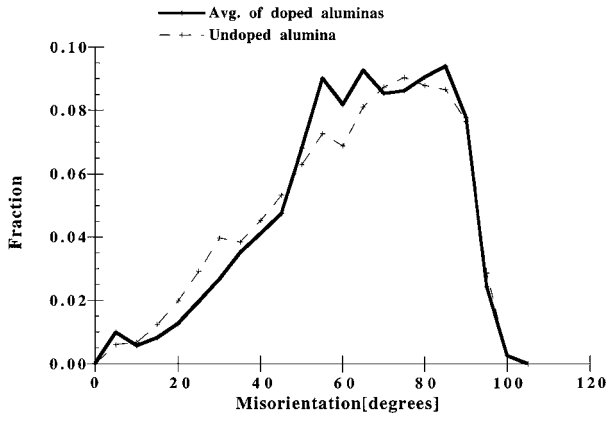

Figure 4 Comparison of misorientation angle distributions between undoped and doped aluminas. The curve from doped aluminas represents the average misorientation distribution of the five doped aluminas.

specimens was plotted as an inverse pole figure (IPF), as shown in Fig. 2. Here, each point is orientation information derived from a single measurement pixel (as opposed to a grain). It is apparent from the IPF that none of the specimens exhibit a very pronounced texture (i.e. preferred orientation). The OIMs from undoped, Y-doped, and La-doped alumina were obtained at the same magnification. Due to the very fine grain sizes of the Nd-doped, Nd/Zr-codoped, and Zr-doped specimens, however, the step size between each measurement during scanning was reduced. Table II summarizes the EBSD acquisition parameters and the specimen grain size.

The distribution of grain boundary misorientation angles for both undoped and doped aluminas is shown in Fig. 3 in the range of 5–55 Å (a), and 55–105 Å (b). In addition, for each misorientation interval, the number fraction for the five doped aluminas were averaged and compared with that of undoped alumina (see Fig. 4). Overall, doping does not seem to have a pronounced influence on the misorientation distribution, although the data suggests a higher proportion of low-angle (<10°) boundaries in the ZR sample. However, it can be seen from Fig. 4 that compared to the undoped alumina, the distribution of grain boundary misorientations of the

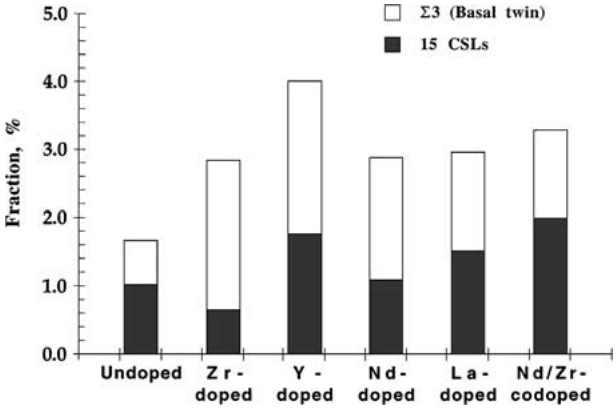

Figure 5 Numerical frequency of selected CSL's for undoped and doped aluminas. A total of 16 CSLs were searched.

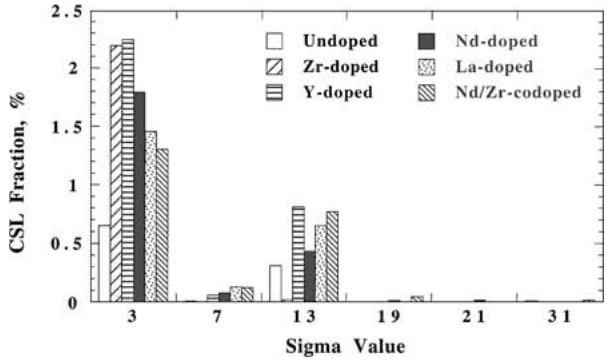

Figure 6 The proportion (by number) of CSL's around the [0001] axis (common rotations with different rotation angles). Note that the basal twin is the only boundary which has a higher incidence for the doped systems.

doped aluminas was slightly skewed towards higher angles ($<50^\circ$).

Selected CSL boundaries (6 CSLs around c-axis and 10 CSLs around the non-c-axis) were searched to test the effect (if any) of these dopants on grain boundary structure in alumina systems. As seen in Fig. 5, the proportion of CSL's was shown to constitute only a small fraction ($<4\%$) of the total number of boundaries. In this case, the permissible angular deviation, θ, from the exact coincidence was determined using Brandon's criterion:

$$\theta = \theta_0/\sqrt{\sum} \tag{2}$$

where θ_0 is a constant ($\sim 15^\circ$) and Σ a multiplicity [25]. The slight increase of total CSLs (about a factor of two) in doped aluminas is mainly due to a higher frequency of $\Sigma 3$ (basal twin) boundaries, as indicated by the open bar histogram in Fig. 5. This increase is the only detectable difference between undoped and doped systems. In contrast, another twin boundary formed on a rhombohedral plane ($\Sigma 7$; 85.90°/[02.1]) was found to be very rare (comprising less than 0.5% of the total number of grain boundaries). Out of interest, the proportion (by number) of basal plane CSL's was identified and plotted in Fig. 6. It can be seen that apart from $\Sigma 3$, the only other boundary present to an appreciable degree was $\Sigma 13$.

Overall, the EBSD results from various doped aluminas revealed only subtle differences in grain boundary misorientation distribution, as compared to undoped alumina. Whether such differences can be attributed to the dopant segregation, or whether they result from other factors such as differences in grain size, the presence of precipitates, etc. requires further study. More significantly, the fraction of special boundaries defined by selected misorientation angle/axis pairs was very limited in the doped aluminas. As mentioned previously, this result (for Y-doped alumina) was also supported by independent work by Gülgün *et al*. [19] on samples provided by Lehigh. These workers used TEM to characterize more than 100 grain boundaries, and found very few special boundaries. This is in marked contrast to the case of Mg-doped alumina which was reported to have around 30% of CSL boundaries [15]. In the present study, the only slight increase in the frequency of special boundaries was for the $\Sigma 3$ (basal twin) boundary. In the Zr-doped and Y-doped systems, there was more than a factor of three increase (relative to undoped alumina); nonetheless, the number fraction of $\Sigma 3$ boundaries was still less than 2.5% of total number of boundaries. It is believed that this small fraction would be insufficient to produce the dramatic creep improvement observed for these compositions.

It should be recognized that in the present study, the CSL information is based solely upon misorientation angle and axis, and the boundary plane is not taken into account. Further, the influence of temperature on the (c/a) ratio was neglected. In the alumina structure, changes in axial ratio, (c/a) can be accommodated by both a deviation in misorientation and a dislocation array. The former may result in the boundary being excluded by giving a value exceeding what would be deduced from Brandon's criterion [26]. In addition, special boundaries consisting of dislocation networks that do not exhibit CSL orientations are not accessible using this technique.

The above considerations notwithstanding, it is believed that the present study shows convincingly that there is little significant difference in the overall grain boundary structure in undoped alumina and doped aluminas. The results, therefore, are consistent with the hypothesis that the improvement in creep behavior results primarily from a lowering of grain boundary diffusion due to a 'site-blocking' effect by the dopant ions, as opposed to increasing the proportion of special boundaries.

4. Summary

In an effort to explain the basic mechanism for creep rate reduction in doped aluminas, we have used the EBSD technique to study a) differences in grain boundary misorientation and b) frequency of selected CSL boundaries between undoped alumina and aluminas doped with oversized dopant ions (Zr, Y, Nd, La, Nd/Zr). It was found that in all cases, the addition of dopant ions produced no significant effect. The only marked change was the increased fraction of $\Sigma 3$ boundary (basal twin) in the doped aluminas, although overall, these CSL boundaries represented only a very small fraction ($<2.5\%$) of the total number. Thus, the work

strongly supports the hypothesis that the beneficial influence of oversized, segregating dopants ions is not primarily through changes in the distribution of grain boundary type and misorientation. Instead, it is argued that the reduction of creep rate occurs by blocking of grain boundary diffusion.

Acknowledgments

This work was supported by the U.S. Air Force Office of Scientific Research (under Contract No. F49620-98-1-0117, monitored by Dr. A. Pechenik). The efforts of Drs. J. D. French, A. M. Thompson, and Mr. G. S. Thompson are gratefully acknowledged for providing some of the alumina specimens.

References

1. J. D. FRENCH, J. ZHAO, M. P. HARMER, H. M. CHAN and G. A. MILLER, *J. Amer. Ceram. Soc.* **77**(11) (1994) 2857.
2. J. CHO, M. P. HARMER, H. M. CHAN, J. M. RICKMAN and A. M. THOMPSON, *ibid.* **80**(4) (1997) 1013.
3. Y.-Z. LI, C. WANG, H. M. CHAN, J. M. RICKMAN, M. P. HARMER, J. M. CHABALA, K. L GAVRILOV and R. LEVI-SETTI, *ibid.* **82** (1999) 1497.
4. E. L. COURTRIGHT, *Ceram. Eng. Sci. Proc.* **12** (1991) 1725.
5. N. M. TALLAN, *ibid.* **12** (1991) 957.
6. B. O. ELFSTRÖM, 3rd Aero Days Post-Conference Proceedings, No. 2 (1998) p. 81.
7. C.-W. LI and W. D. KINGERY, in "Advances in Ceramics," Vol. 10, Structure and Properties of MgO and Al_2O_3 Ceramics, edited by W. D. Kingery (American Ceramic Society, Columbus, OH, 1984) p. 368.
8. M. K. LOUDJANI, A. M. HUNTZ and R. CORTES, *J. Mater. Sci.* **28** (1993) 6466.
9. A. M. THOMPSON, K. K. SONI, H. M. CHAN, M. P. HARMER, D. B. WILLIAMS, J. M. CHABALA and R. LEVI-SETTI, *J. Amer. Ceram. Soc.* **80**(2) (1997) 373.
10. J. BRULEY, J. CHO, J. C. FANG, A. M. THOMPSON, Y. Z. LI, H. M. CHAN and M. P. HARMER, *ibid.* **82** (1999) 2865.
11. J. CHO, Ph. D. thesis, Lehigh University, 1998.
12. H. YOSHIDA, Y. IKUHARA and T. SAKUMA, *Phil. Mag. Lett.* **79** (1999) 249.
13. H. KOKAWA, T. WATANABE and S. KARASHIMA, *Phil. Mag. A* **44**(6) (1981) 1239.
14. S. LARTIGUE and L. PRIESTER, *J. Amer. Ceram. Soc.* **71**(6) (1988) 430.
15. *Idem., J. Physique* **C5-49** (1988) 451.
16. S. LARTIGUE-KORINEK and F. DUPAU, *Acta Met.* **42** (1994) 293.
17. D. BOUCHET, F. DUPAU, F. and S. LARTIGUE-KORINEK, *Microsc. Microanal. Microstruct.* **4** (1993) 561.
18. J. CHO, H. M. CHAN, M. P. HARMER and J. M. RICKMAN, *J. Amer. Ceram. Soc.* **81**(11) (1998) 3001.
19. M. A. GÜLGÜN, V. PUTLAYEV and M. RÜHLE, *ibid.*, in press.
20. D. J. DINGLEY and V. RANDLE, *J. Mater. Sci.* **27** (1992) 4545.
21. S. J. WRIGHT and B. L. ADAMS, *Metall. Trans. A* **23** (1992) 759.
22. J. CHO, C. WANG, H. M. CHAN, J. M. RICKMAN and M. P. HARMER, *Acta. Met. et. Mat.* **47** (1999) 4197.
23. V. RANDLE, "Microtexture Determination and Its Applications" (The Institute of Materials, London, 1992).
24. H. GRIMMER, R. BONNET, S. LARTIGUE and L. PRIESTER, *Phil. Mag. A* **61**(3) (1990) 493.
25. D. G. BRANDON, *Acta Metall.* **14** (1966) 1479.
26. K. SHIN and A. H. KING, in "Structure and Property Relationships for Interfaces," edited by J. L. WALTER, A. H. KING and K. TANGRI (ASM International, 1991) p. 25.

Received 14 March
and accepted 4 September 2001